ASAR product consistency and geolocation accuracy

Schubert, A ; Small, David ; Miranda, N ; Meier, E

Abstract: The ability to geolocate ENVISAT ASAR image products and transform them into a map projection is a critical step required to enable not only overlays with other sources of information (e.g. DEM, GIS layers), but even with other ASAR products, especially those acquired with a different track, beam, or incidence angle. This paper summarises geolocation validation results evaluating both the relative (i.e. consistency within product families) and absolute geolocation accuracy inherent to ASAR products generated by the ESA operational processor (PF-ASAR). A set of slant-range complex IMS/APS/WSS-, ground-range detected IMP/APP-, IMM/APM/WSM-, and ellipsoid-geocoded detected IMG/APG products were ordered for a set of data takes over the Netherlands (IM AP) and Switzerland (WS products). Subswath detection and mosaicking was performed on the WS-SLC (WSS) products to enable their comparison with WSM products derived from the same raw data. All products were then ellipsoid-geocoded to permit direct intercomparisons. To quantify the small relative shifts between the product types, a dense image matching algorithm was used to compare geocoded ellipsoid-corrected (GEC) product pairs. Statistical analysis (mean, standard deviation) of the resulting disparity fields revealed processor biases, and enabled improvement of the PF-ASAR processor. WSS/WSM comparisons revealed slight beam-dependent relative azimuth shifts of up to 19 m, well below the native WSM sample spacing of 75 m. Radiometric differences between WSS and WSM products were also evaluated point by point in the ellipsoid-geocoded map geometry, and revealed a possible error in the AGP calibration for WSS products. For some data sets, the absolute geolocation accuracy was measured using transponders with well-known locations, prominently visible in the ASAR products. Both range-Doppler- and geolocation grid-based geolocation was performed for the in-scene transponders. A given predicted position was then compared to the measured position obtained through direct observation of a strong peak response in the neighbourhood of the prediction. ASAR products were generally found to be extremely consistent with respect to each other, with measured relative differences all at the sub-sample level. An intermittent range bias is the one remaining source of large geolocation error, although it has not yet been observed in images acquired since 2006. ASAR's absolute geolocation accuracy has set a new standard for spaceborne SAR sensors. ASAR was the first operational spaceborne SAR imager to provide data that can (generally) be geolocated without the use of tie-pointing.

ASAR Product Consistency and Geolocation Accuracy

Adrian Schubert[(1)], David Small[(1)], Nuno Miranda[(2)], Erich Meier[(1)]

[(1)] Remote Sensing Laboratories, University of Zürich
Winterthurerstrasse 190; CH-8057 Zürich, Switzerland
Email: {Adrian.Schubert, David.Small, Erich.Meier}@geo.uzh.ch

[(2)] European Space Agency - ESA-ESRIN
Via Galileo Galilei, I-00044 Frascati, Italy
Email: Nuno.Miranda@esa.int

ABSTRACT

The ability to geolocate ENVISAT ASAR image products and transform them into a map projection is a critical step required to enable not only overlays with other sources of information (e.g. DEM, GIS layers), but even with other ASAR products, especially those acquired with a different track, beam, or incidence angle. This paper summarises geolocation validation results evaluating both the relative (i.e. consistency within product families) and absolute geolocation accuracy inherent to ASAR products generated by the ESA operational processor (PF-ASAR).

A set of slant-range complex IMS/APS/WSS-, ground-range detected IMP/APP-, IMM/APM/WSM-, and ellipsoid-geocoded detected IMG/APG products were ordered for a set of data takes over the Netherlands (IM & AP) and Switzerland (WS products). Subswath detection and mosaicking was performed on the WS-SLC (WSS) products to enable their comparison with WSM products derived from the same raw data. All products were then ellipsoid-geocoded to permit direct intercomparisons.

To quantify the small relative shifts between the product types, a dense image matching algorithm was used to compare geocoded ellipsoid-corrected (GEC) product pairs. Statistical analysis (mean, standard deviation) of the resulting disparity fields revealed processor biases, and enabled improvement of the PF-ASAR processor.

WSS/WSM comparisons revealed slight beam-dependent relative azimuth shifts of up to 19 m, well below the native WSM sample spacing of 75 m. Radiometric differences between WSS and WSM products were also evaluated point by point in the ellipsoid-geocoded map geometry, and revealed a possible error in the AGP calibration for WSS products.

For some data sets, the absolute geolocation accuracy was measured using transponders with well-known locations, prominently visible in the ASAR products. Both range-Doppler- and geolocation grid-based geolocation was performed for the in-scene transponders. A given *predicted position* was then compared to the *measured position* obtained through direct observation of a strong peak response in the neighbourhood of the prediction.

ASAR products were generally found to be extremely consistent with respect to each other, with measured *relative* differences all at the sub-sample level. An intermittent range bias is the one remaining source of large geolocation error, although it has not yet been observed in images acquired since 2006.

ASAR's absolute geolocation accuracy has set a new standard for spaceborne SAR sensors. ASAR was the first operational spaceborne SAR imager to provide data that can (generally) be geolocated without the use of tie-pointing.

INTRODUCTION

The algorithms chosen within ESA's PF-ASAR processor can vary depending on product type: geometric differences between products based on the same acquisition can occur. Placing all product types in one consistent geometry would allow evaluation of systematic shifts.

Absolute geolocation accuracies were measured by comparing predicted to measured target locations in the images. Using oversampling, the locations of special targets such as transponders or corner reflectors may be measured to subpixel accuracy. The location of a target's *predicted* location varies depending on the geolocation algorithm applied to make the estimation as well as the input parameters. Those parameters include the type of state vectors used, as well as the radar timing annotations (both in the range and azimuth dimensions) that accompany any ASAR product.

Four different state vector product types are available: precise, preliminary, restituted, and predicted (in decreasing order of quality). Each state vector product type provides estimates of the satellite's position and velocity within a given time interval. Any may be used to reconstruct the satellite's orbit at the time of acquisition of a given SAR image. During typical range-Doppler (RD) geolocation, one solves the Doppler equation governing a given SAR image product's

geometry, searching for the azimuth time where the satellite's position corresponds to the required Doppler value (typically zero).

A more simplified geolocation method makes use of the geolocation grid (GG) provided in ENVISAT ASAR products (Location Annotation Data Set – LADS), retrieving the range and azimuth times of a given target via bicubic interpolation between the corresponding values at latitude/longitude grid points provided. However, the grid is extremely coarse, typically 11x11 points distributed across the scene, and is calculated using a *single* reference height.

The image matching algorithm used in this work is based on a complex wavelet decomposition of the input images, and is described in [1] and [2]. It effectively combines area- and feature-based matching methods. The disparities are estimated for each sample position and are given as separate horizontal and vertical components.

METHODOLOGY

A set of slant-range (SLC) IMS/APS, ground-range IMP/APP/IMM/APM, and ellipsoid-geocoded (GEC) IMG/APG products were ordered for a set of data takes over the Netherlands for geometric inter-comparison.

PF-ASAR products presented in radar geometry (IMS/APS, IMP/APP, IMM/APM) were ellipsoid-geocoded to a common UTM map geometry using common precise state vectors and the map projection and datum shift parameters annotated in the corresponding IMG/APG products. The geocoding was performed by solving the range-Doppler equations for each raster location in the input ellipsoid height model, and resampling the backscatter from radar geometry (slant or ground) into the ellipsoid map geometry. Bistatic correction [4] was (exceptionally) *not* applied during geocoding, in order to best "simulate" the IMG/APG product generation process, maximising their agreement with IMG and APG products, which do not have the azimuth bias corrected. The resulting "IMS/APS-GEC", "IMP/APP-GEC", and "IMM/APM-GEC" (Geocoded Ellipsoid Corrected) images were then compared to each other and to the corresponding IMG/APG product for each acquisition.

To better quantify the smaller relative shifts between the product types, an image matching algorithm [1] [2] was used to compare "GEC" product pairs. For each orbit, six pairs were matched against each other: the geocoded product produced by PF-ASAR (IMG or APG) versus the three slant- and ground-range images, and the slant-ground images versus each other. All output grid spacings were set to the 12.5 metres defined in the IMG/APG products.

The estimated shifts, or disparities, were stored as horizontal and vertical (easting and northing) components. The procedure used for product comparison is summarised graphically in Fig. 1.

Histograms of the disparity fields were calculated for all "GEC" image pairs, as well as the mean and standard deviations. Because the *mean* value of a disparity field is only significant when the measured relative shift is approximately constant across the scene, the vector field images were first inspected for trends. In all cases studied, the disparity fields were seen to be either constant or random, the latter indicative of pure matching noise (no significant relative shift detected). In such cases, the mean disparity can be assumed to be valid for the entire image pair in question, with the standard deviation reflecting the "confidence" with which the mean can be said to apply.

Following the IM/AP experiments, several WSS and WSM products were ordered to test the geometric as well as radiometric consistency within the "WS" product family.

The WSS products were first mosaicked [3], providing single slant-range images that could be geocoded. The resulting "WSM-GEC" and "WSS-GEC" (Geocoded Ellipsoid Corrected) images were then compared to each other using the same complex-wavelet image matching algorithm [1] [2] applied in the IM/AP comparisons.

The procedure followed for each of five WSM/WSS pairs is illustrated in Fig. 2. Mosaicking [3] was first performed on all WSS products (see Fig. 2a). The native ground range pixel spacing of WSM products is 75 m. The WSS mosaics were generated using a range multi-looking factor of six, producing a mosaic slant range sample spacing of 47 m and an azimuth spacing of 80 m, "optimising" for approximately square ground range samples at the scene centre.

Backward ellipsoid geocoding was then applied to both the WSM and mosaicked WSS products (see Fig. 2b), as described earlier for the IM and AP products. Image matching and calculations of statistics were performed as well. A rectangular matching window was chosen for each pair manually to ensure inclusion of data from all five WS subswaths without extending into "null cell" boundary regions.

Subswath-dependent effects were further investigated by comparing a mosaic of one of the WSS products to a radiometric simulation of the mosaic [5]. The image simulation was based on a DEM, the satellite state vectors, and the mosaic's timing annotations. The image simulation is not influenced by the location of beam-boundaries, since it has no knowledge of the sub-swath positions. Comparing the simulated image to the mosaic was therefore useful to detect possible geometric shifts at beam boundaries in the WSS product and mosaic.

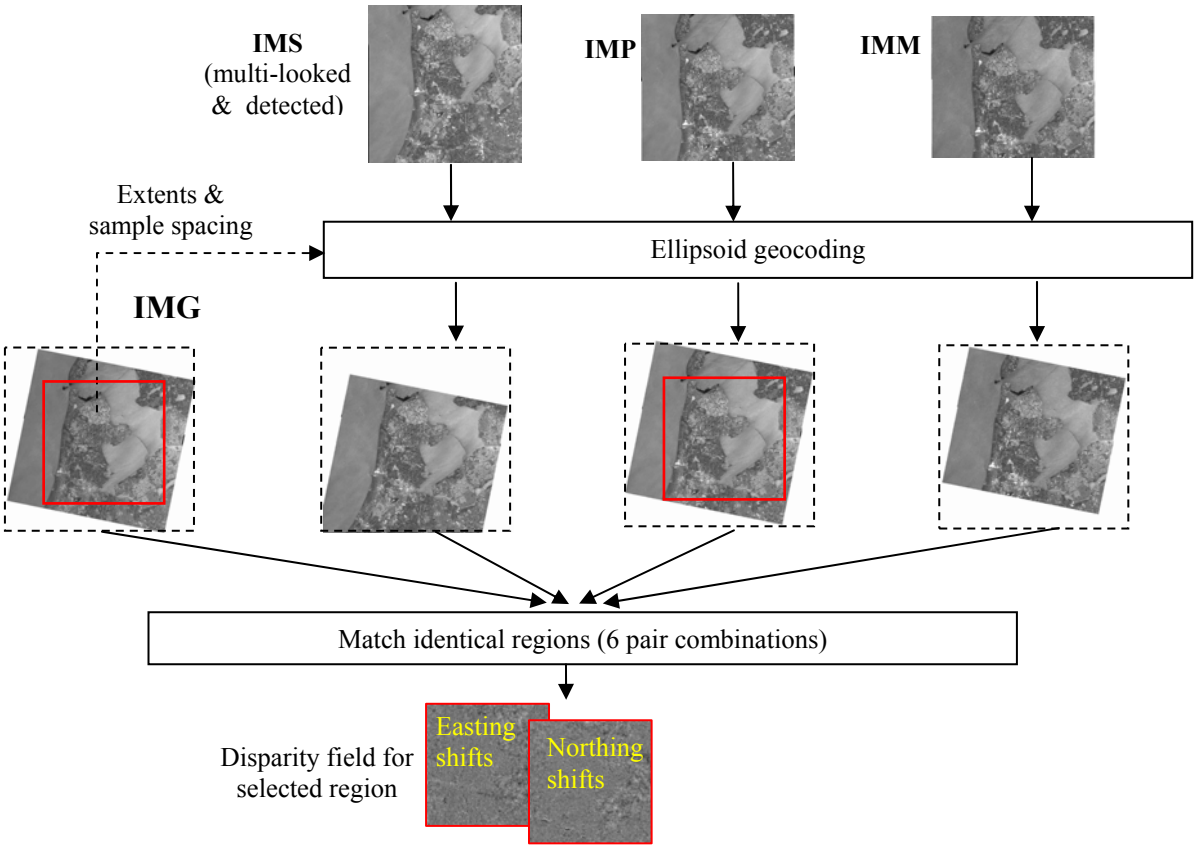

Fig. 1 Procedure followed for IMG/IMS/IMP/IMM comparisons (shifts between IMG and IMP highlighted here)

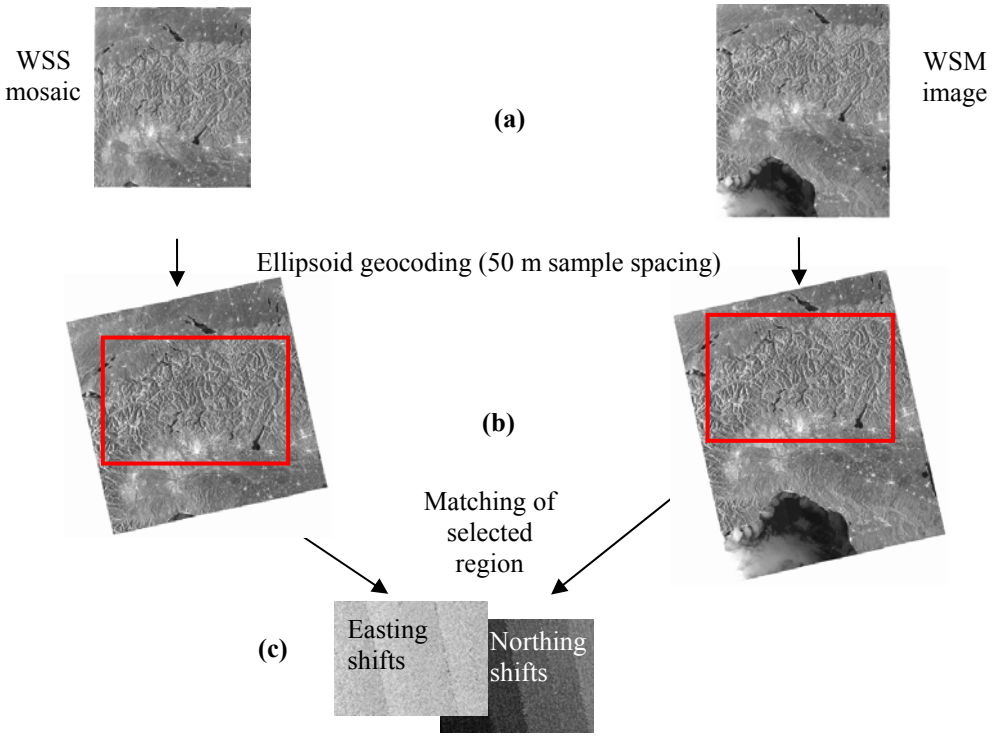

Fig. 2 Procedure followed for WSM/WSS comparison: (a) Generation of mosaicked (WSS) and detected (WSM) images, (b) ellipsoid geocoding to a common geometry, and (c) matching of selected common region, with separate results for horizontal and vertical (easting and northing) shifts, in 50 m sample units.

The WSS-GEC and WSM-GEC images in common map geometries were compared radiometrically to test for product consistency. The difference was expressed in decibels by calculating $10 \cdot \log_{10}$ of the backscatter ratio (WSS/WSM).

In preparation for measurements of *absolute* geolocation accuracy, a total of 108 IM, AP, and WS data sets were acquired over transponders in Canada and Netherlands, and both RD- and GG-based geolocation was performed for the transponder known to be within each given scene. The *predicted position* so obtained was then compared to the *measured position* obtained through direct observation of a strong peak response in the neighbourhood of the prediction. The range and azimuth differences Δr and Δa between *predicted* (p) and *measured* (m) transponder positions were calculated for `AUX_FPO`, `AUX_FRO`, `DOR_POR`, `DOR_VOR`, and `LADS` estimation methods:

$$\Delta r = r_p - r_m \qquad \Delta a = a_p - a_m$$

RESULTS AND DISCUSSION

RELATIVE GEOLOCATION ACCURACY

All four IM and AP product types were ordered for nine orbits covering the Flevoland area in the Netherlands. SLC products from three orbits had previously been observed to have range biases of up to 20 samples [6]. All product types were subsequently ordered for these orbits. As "pathological" cases were explicitly sought for the study, it is important to note that the rate of intermittent range bias occurrence is not representative of the rate within the archive as a whole.

The matching results are given as relative horizontal and vertical shifts in 12.5 m sample units. Although the medium-resolution images have original sample spacings of 75 m, they were resampled to 12.5 m in the GEC UTM geometry during geocoding in preparation for image matching. Vertical shifts are mainly – but not entirely - due to azimuth timing errors, while horizontal shifts are caused primarily by range errors, since scene headings are typically ~16° relative to north-south at this latitude. The means and standard deviations of the shift estimates were calculated for the match window in all cases, after verifying that no noticeable trends or rotations were measured.

Table 1 summarises the relative shift statistics for all tested products *excluding* those with known biases (discussed below). Two general cases can be distinguished: (1) Geocoded (IMG/APG) versus PRI (IMP/APP) products have the smallest relative shifts, with standard deviations under $1/10^{th}$ of a sample. This is unsurprising, as IMG/APG products are derived internally within PF-ASAR from IMP/APP images, respectively. (2) All *other* product comparisons have standard deviations on the order of ~$1/5^{th}$ to ~$1/6^{th}$ of a *native* sample. When medium-resolution images (MRIs, namely IMM/APM) are being matched (N.B. their native sample spacing is 75 m), the measurement noise is proportionally higher. This can be seen in the table: the standard deviations are either on the order of ~0.2 samples or ~1.1 samples, where the reference sample spacing is 12.5 m. Overall, products derived from the same acquisition are extremely consistent, with no noticeable trends.

When present, the intermittent range bias effect [5] contributes the largest relative shifts; we observed shifts of up to 19 easting and 6 northing samples, corresponding to ~20 slant-range samples. As described in [5] and [6], all PF-ASAR products subject to large observed range biases were generated using the RD input chain, while a separate chain built around products that use the SPECAN algorithm is used for those product types that appear to be "immune" to large range biases. This indicates a possible intermittent problem in the RD input chain. Detailed analyses of this problem were included in [7]. Note that this problem was only rarely observed, and has not been seen in products acquired since 2006.

Table 1 Relative shift statistics (estimates of mean ± standard deviation) for ellipsoid-geocoded IM and AP products, *excluding* products with intermittent range bias and medium-resolution-ascending anomalies. Indicated offset values transform the "slave" into the reference geometry. Units: [12.5-metre *samples*].

Reference product type	**IMG & APG**			**IMS- & APS-GEC**		**IMP- & APP-GEC**
Slave product type	**IMS- & APS-GEC**	**IMP- & APP-GEC**	**IMM- & APM-GEC**	**IMP- & APP-GEC**	**IMM- & APM-GEC**	**IMM- & APM-GEC**
Easting	-0.02±0.22	-0.03±0.06	-0.22±1.06	0.01±0.21	-0.04±1.04	-0.04±1.04
Northing	0.04±0.22	0.04±0.09	-0.25±1.05	0.02±0.22	-0.40±1.06	-0.30±1.09

A second much smaller effect is observed in the match results involving medium-resolution images (IMM/APM, both SPECAN-processed) acquired from ascending orbits; shifts of ~15 m were typical. While this is a sub-pixel effect for medium-resolution images, it seems to appear with regularity. While much less significant than the intermittent range bias issue, it remains worthy of further investigation. Detailed statistics for all product pairs were reported in [7].

The processing chain illustrated in Fig. 2 was applied to five available WSM/WSS product pairs covering Switzerland. Table 2 lists the measured mean relative shifts and standard deviations for two typical examples – results are provided in units of [50 m samples] as well as [m]. Visualisations of the geometric distributions of the shift values are shown in the right-most column. They were all linearly scaled using the same limits (-0.6 to +0.6 samples), a range selected to include the shifts for *all* results.

In all cases studied, the mean shift values range from about 0 to 16 metres, well below the native WSM and WSS ground-range sample intervals (75 m and ~80 m, respectively). Note also that the magnitude of the shift is slightly beam-dependent, as the images in the right-hand column of the table indicate. Furthermore, the variation from beam to beam follows a consistent pattern for all ascending and all descending pairs. Regarding the entire scene, the northing shift components dominate in all cases, indicating mainly azimuth-related effects. In particular, the two ascending-orbit product pairs exhibit noticeably strong negative relative easting and northing shifts, pointing to a possible systematic offset between the ascending WSM and WSS pairs.

In order to better quantify the small beam dependency seen in the match results, a measurement window of constant size was used to quantify the shift statistics for each beam separately. For one product pair, Table 3 lists the individual shifts estimated within each sub-swath (beam). A window of constant size was placed over data from each beam, and the statistics calculated for both the horizontal (easting) and vertical (northing) shift images. As would be expected after reviewing the images in Table 2, the standard deviations are reduced in comparison to appraisals that encompass the entire image.

Given that consistent beam-dependent biases clearly exist in the WSM/WSS comparisons, possible sources are worthy of investigation. The fact that relative shifts between WSM/WSS appear to be much stronger for ascending pairs than descending pairs should also be considered. A possible answer to the latter point may be attribution of the ascending results to the "ascending medium-resolution anomaly" observed for the IMM/APM products. It was seen that ascending medium-resolution products were offset by up to 14 m in the easting direction and up to -13 m in the northing direction, similar to what we observe in Table 2 for orbit 31188. It therefore seems likely that the particularly high relative shifts seen in the WSM/WSS comparisons are mainly due to the same "ascending medium-resolution" anomaly that is not yet well understood.

In an attempt to determine the source of the observed beam-dependent relative shifts between WSM-GEC and WSS-GEC products, *simulated* images [5] of each of one of the WSS mosaics and one of the WSM products were compared to the real images, again using image matching. The simulations were synthesised using orbital and timing annotations generated during WSS mosaicking. A 25 m resolution Swiss digital height model was traversed, and the local illuminated area was estimated in the WSS-mosaic slant-range geometry.

Table 2 Relative shifts (mean ± standard deviation) for 2 ellipsoid-geocoded WS products. Indicated offset values transform the WSM-GEC into the WSS-GEC geometry.

		50 m Samples	Metres	Linearly scaled visualisations (saturated endpoints) (black = -0.6 sample, white = +0.6 sample)
Descending Orbit 18026	Easting	0.03 ± 0.23	1.3 ± 11.7	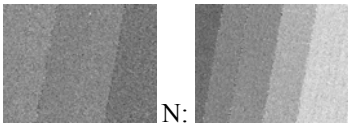
	Northing	0.13 ± 0.24	6.6 ± 12.2	
Ascending Orbit 31188	Easting	0.30 ± 0.28	14.9 ± 14.0	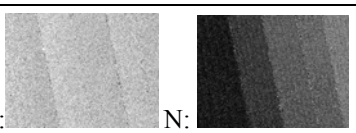
	Northing	-0.25 ± 0.29	-12.4 ± 14.5	

Table 3 WSM/WSS relative shifts (mean ± standard deviation) measured within *each sub-swath* for descending orbit 18026 (acquired 2005.08.11). A rectangular sub-window of constant size (697 x 2121 samples) was analysed for shift data from each sub-swath.

	Easting		Northing	
	50 m Samples	Metres	50 m Samples	Metres
SS1	-0.04 ± 0.19	-2.0 ± 9.7	0.38 ± 0.17	19.2 ± 8.3
SS2	0.04 ± 0.18	1.8 ± 8.9	0.21 ± 0.15	10.6 ± 7.5
SS3	0.02 ± 0.18	0.8 ± 8.9	0.06 ± 0.15	3.1 ± 7.3
SS4	0.07 ± 0.19	3.3 ± 9.7	0.02 ± 0.15	1.2 ± 7.6
SS5	0.06 ± 0.19	3.1 ± 9.6	-0.09 ± 0.16	-4.5 ± 7.9

The measurement noise in the simulation-versus-real comparisons was higher (14 m in range, 28 m in azimuth) than for the real-versus-real matching because of the lack of a groundcover-dependent signal in the simulations. The inter-beam azimuth variations of < 8 m measured in the real-versus-real cases was probably therefore undetectable. However, the simulated-versus-real comparisons confirm broadly consistent geometries in the WSS/WSM products. Indeed, the WSS/WSM comparisons (Table 2 and Table 3) show that although visible when properly scaled, beam-boundary shifts were never greater than ~8 m (N.B. ~0.15 samples).

RADIOMETRIC COMPARISON OF WSS AND WSM PRODUCTS

The relative geometric consistency between WSS/WSM products was evaluated in the previous section, which required geocoding them to a common reference geometry. The common geometry also enables relatively straightforward *radiometric* comparisons. The independent calibration of the individual beams in WS products makes such comparison of particular interest. The respective products are produced by significantly different input and processing chains (WSM: SPECAN, WSS: Range-Doppler).

A given target's backscatter within a WS acquisition should be identical when retrieved from either a WSS or WSM product. We calculated the log-differences 10 $\log_{10}$(WSS) - 10 $\log_{10}$(WSM) for 13 pairs of WSM/WSS products acquired between 2004 and 2008 over Switzerland, Canada, and Brazil. In all 13 cases, a distinctive beam-dependent range pattern was seen; a typical result is shown in Fig. 3 for a Switzerland ascending scene acquired on February 13, 2008. The WSM and mosaicked WSS products are shown on the left; both were geocoded to a common geometry; the area common to both (in red) was used for the log-difference calculation. On the right, the "difference image" is shown scaled from -1.5 dB (black) to +1.5 dB (white).

The most noticeable effect in all 13 cases investigated, including Fig. 3, is a smoothly-varying brightness pattern ("ripples") in the range direction, typically with local maxima occurring within each subswath. The effect is often strongest for beams SS1 through SS3, with clearly visible "wave crests" within each of them.

The difference image from a descending pass over Switzerland is shown in Fig. 4, along with the associated histogram. Two further artefacts are apparent in the difference images as well. As can be seen in Fig. 3 and Fig. 4, a regular azimuth pattern (dark, narrow bands of noise) can appear as well as strong brightness variations at the subswath boundaries. While the swath boundary errors suggest differences in the respective mosaicking WSS/WSM algorithms, the cause of the azimuth pattern is not yet understood.

It is possible that the "ripples" in the WSS/WSM differences may be due to beam calibration errors in WSS products caused by an erroneous scene height annotation. Both the WSS and WSM product annotations contain a parameter describing the average scene height above the ellipsoid; for WSM products, a realistic terrain height is annotated, whereas all WSS products encountered to date have this parameter set to zero. The parameter may be used for modelling the elevation antenna gain pattern (AGP), implying that AGP differences could be the cause of the "ripple" pattern in the log-differences.

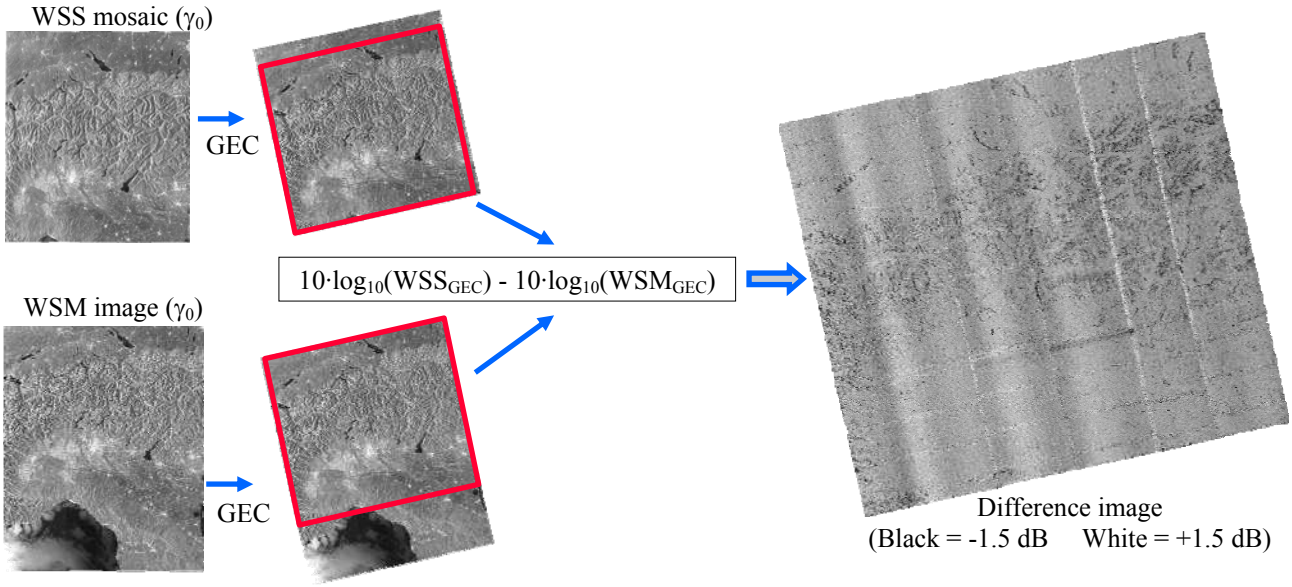

Fig. 3 Log-difference between WSS and WSM backscatter

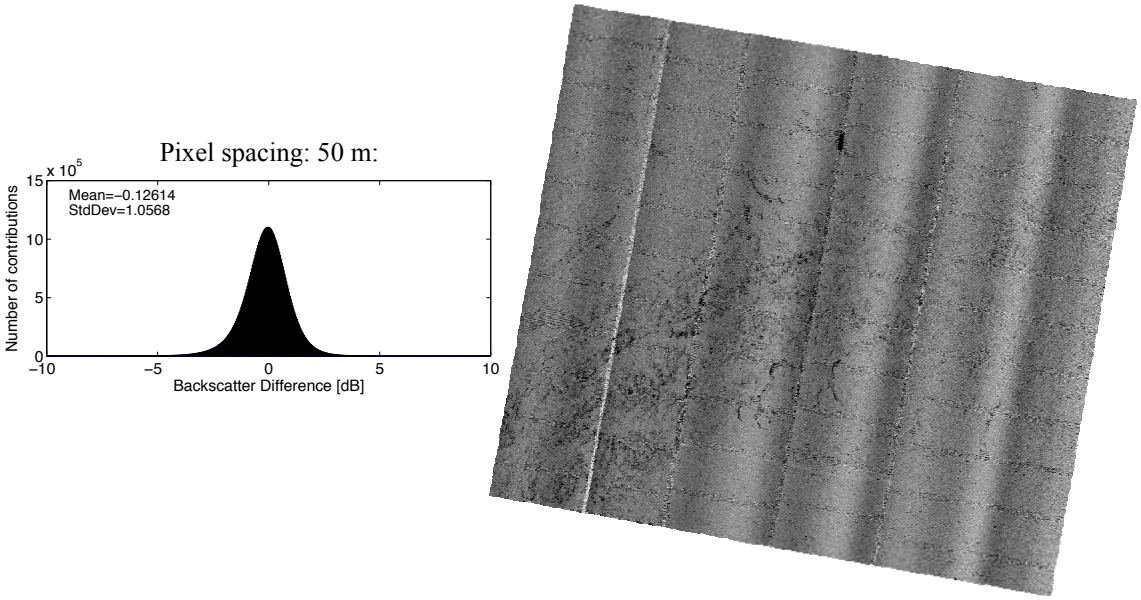

Fig. 4 ($10 \cdot \log_{10}$WSS - $10 \cdot \log_{10}$WSM) for Switzerland (Desc orbit 18026). Black = -1.5 dB White = +1.5 dB

ABSOLUTE GEOLOCATION ACCURACY

Scatter plots were calculated indicating the geolocation accuracy obtained using the five investigated geolocation methods (RD with predicted, restituted, preliminary, and precise orbits, as well as GG-based interpolation). As an example, for the results from the Edam and Resolute ASAR transponders, scatter plots showing the geolocation accuracy achieved for image mode products using precise state vectors (`DOR_VOR`) are shown together in greater detail in Fig. 5. Note that although the geolocation accuracies are generally high, a unique "residual inaccuracy" is apparent at each transponder site. A small single-digit metre survey inaccuracy might be causing the pattern seen for the Edam transponder (Fig. 5a).

Comparing Fig. 5c and d, note also that the *prima facie* poorer location measurement accuracy for IMP products as compared to the equivalent higher-resolution IMS products is only an expression of the ground-range projection (IMP) versus the slant-range geometry (IMS). In Fig. 5b one sees that the range geolocation estimate is extremely consistent, also between ascending and descending datasets.

Quantitative geolocation accuracy results for IM & AP products are summarised more compactly in Table 4. Note that the values indicate the geolocation accuracy achieved *without* the use of any tiepoints. Especially high accuracy is emphasised with green colouring, particularly poor accuracy is marked with red. Within the table, the column "Transponder" indicates the number and type of transponders present in the scenes; the "Products" column lists the number and type of products investigated. For all the IMS & IMP products listed, a single transponder was present within each product. In the case of the APS product study, multiple ASAR transponders were present: eight APS products were investigated, encompassing twelve transponder measurements.

The absolute location error (ALE) estimates are listed as RMS values in metres. Note that restituted, preliminary, or precise state vector based geolocation are all preferable to the GG or predicted state vector based methods. Also, for slant range products (IMS, APS) the ALE is expressed as a combination of azimuth and *slant* range error, while for ground range products (IMP) the ALE combines azimuth and *ground* range error. The IMS/IMP results for the Resolute transponder are shaded with the same grey to indicate that they derive from the same ASAR IM data acquisitions.

Note that transponder-specific range and azimuth biases caused by, for example, survey error, contribute to these RMS values. Fig. 5(a) shows probable survey error affecting the measurements. If the transponder reference GNSS survey positions could be improved, it is expected that the retrieved *geolocation accuracies would also improve*. Indeed, the achievable agreement between predicted and measured positions currently appears to be limited by the quality of the transponder GNSS surveys and not the radar data itself.

The quantitative geolocation accuracy results for WSM products derived from WS acquisitions over Resolute and Edam are summarised in Table 5. Previous similar investigations for WSS products using RADARSAT transponders in Canada showed that measured locations were usually within 10 m of the predictions [3]. Table 5 shows again that geolocation based on restituted, preliminary, or precise state vectors is preferable to state vector models based on predicted-quality (`AUX_FPO`) state vectors. Note that although the tabulated results were all achieved *without* the use of any tiepoints, the prediction geolocation accuracies are generally within one third of a WSM product sample, often better. Transponder-specific range and azimuth biases (e.g. medium resolution azimuth anomaly) are included within the WSM-product geolocation errors. As in the IM and AP cases, a more accurate survey of the transponder reference survey positions would likely improve the geolocation accuracies obtained.

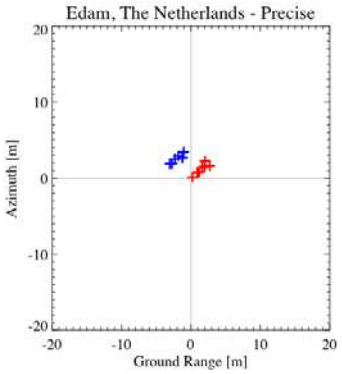

(a) IMP Edam transponder, The Netherlands

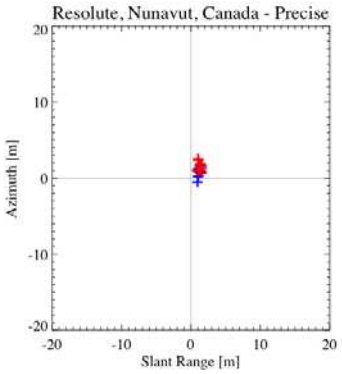

(b) IMS 2004 Resolute RSAT transponder, Nunavut, Canada

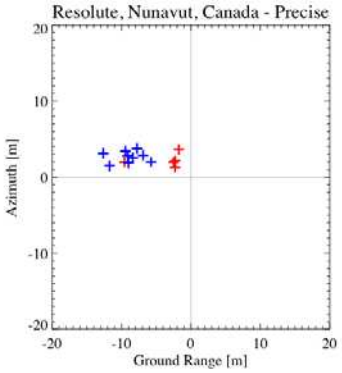

(c) IMP 2007-8 Resolute ASAR transponder, Nunavut, Canada

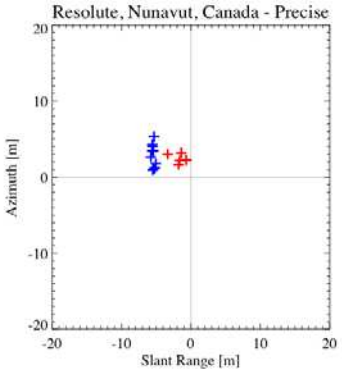

(d) IMS 2007-8 Resolute ASAR transponder, Nunavut, Canada

Fig. 5 Summary of Transponder DORIS Precise-orbit-based Absolute Geolocation Accuracies for IMS/IMP Products

Table 4 Transponder RMS Absolute Location Error for IM & AP Products [m]

Site	Transponder	Products	Date Range	LADS	Predicted	Restituted	Preliminary	Precise
Resolute	1 RSAT	19 IMS	2004-2006	14.8	16.0	2.4	1.8	1.8
	1 ASAR	14 IMS	2007-2008	12.3	15.6	5.4	5.5	5.5
	1 ASAR	14 IMP	2007-2008	19.9	21.0	8.1	8.3	8.3
NL	1 ASAR (Edam)	15 IMP	2007-2008	81.7	18.9	2.9	2.7	2.7
	3 ASAR	8* APS	2003-2005	30.8	214.7	4.4	4.0	4.0

* 12 measurements from Edam, Zwolle, and Aalsmeer transponders

Table 5 Transponder RMS Absolute Location Error for WSM Products [m]

Site	Transponder	Products	Date Range	LADS	Predicted	Restituted	Preliminary	Precise
Resolute	1 RSAT	11 WSM	2004-2006	X	21.4	12.0	12.0	12.0
Edam	1 ASAR	10 WSM	2005-2008		24.5	24.7	25.8	25.8

CONCLUSIONS

The broad spectrum of ASAR products was found to generally be extremely consistent, with measured *relative* shifts all at the sub-sample level. Improved transponder surveys would almost certainly enable higher achievable *absolute* geolocation accuracies.

An intermittent range bias [5] is the one remaining source of large geolocation error. Although it has not yet been observed in images acquired since 2006, it warrants further investigation to improve the worst-case geolocation accuracy to be expected from the contents of the ASAR archive.

A small but consistent sub-sample bias was observed for medium-resolution products acquired from ascending orbits. Although its effect is small, its regularity makes it worthy of further investigation.

A possible ellipsoid height annotation error causing AGP miscalibration may be largely responsible for differences up to 1.5 dB observed between WSM and WSS product backscatter values. Users performing radiometric investigations should generally keep to one product type, especially in areas with steep terrain.

ASAR's absolute geolocation accuracy has set a new standard for spaceborne SAR sensors. ASAR was the first operational spaceborne SAR sensor providing data than can (generally) be geolocated without the use of tie-pointing.

REFERENCES

[1] Magarey J. and Dick A., *Multiresolution stereo image matching using complex wavelets*, Proc. Intl. Conference on Pattern Recognition, Vol. 1, No. 14, 1998, pp. 4-7.

[2] Schubert A., Small D., Meier E., Nüesch D., *Extraction of Surface Topography from SAR Images Using Combined Interferometry and Stereogrammetry*, Proc. EUSAR 2004, Ulm, Germany, May 25-27, 2004, pp. 775-778.

[3] Schubert A., Small D., Rosich B., Meier E., *ASAR WSS Product Verification Using Derived Image Mosaics*, Proc. Envisat Symposium 2007, Montreux, Switzerland, April 23-27, 2007 (ESA SP-636, July 2007), 6p.

[4] Small D., Rosich B., Schubert A., Meier E., Nüesch D., *Geometric Validation of Low and High-Resolution ASAR Imagery*, Proc. ENVISAT & ERS Symposium 2004, Salzburg, Austria, Sept. 6-10, 2004 (ESA SP-572, April 2005). 9p.

[5] Small D., Schubert A., Rosich B., Meier E., *Geometric and Radiometric Correction of ESA SAR Products*, Proc. Envisat Symposium 2007, Montreux, Switzerland, Apr. 23-27, 2007 (ESA SP-636, July 2007), 6p.

[6] Small D., Rosich B., Schubert A., Meier E., *ENVISAT ASAR Geometric Validation*, Proc. CEOS CAL/VAL Workshop, Oct. 3-6 2006, Edinburgh, Scotland.

[7] Small D., Schubert A., *ASAR Geolocation Accuracy*, ESA Report Reference RSL-ASAR-GC-ACC, Issue 1.0, June 24, 2008.